IEEE Access
Multidisciplinary | Rapid Review | Open Access Journal

Received July 12, 2019, accepted August 10, 2019, date of publication August 16, 2019, date of current version August 29, 2019.

Digital Object Identifier 10.1109/ACCESS.2019.2935770

Real-Time Diagnosis of an In-Wheel Motor of an Electric Vehicle Based on Dynamic Bayesian Networks

HONGTAO XUE, (Member, IEEE), JIAWEN ZHOU, ZHENYU CHEN, AND ZHONGXING LI
School of Automotive and Traffic Engineering, Jiangsu University, Zhenjiang 212013, China

Corresponding author: Hongtao Xue (xueht@ujs.edu.cn)

This work was supported in part by the National Natural Science Foundation of China under Grant 51775245, in part by the China Postdoctoral Science Foundation under Grant 2016M601740, and in part by the Primary Research and Development Plan of Jiangsu Province under Grant BE2017129.

ABSTRACT This study proposes a new real-time diagnosis method for an in-wheel motor (IWM) of an electric vehicle (EV) based on dynamic Bayesian networks (DBNs). Since the electrical signal of the vehicle power supply is unstable because of the interference resulting from the EV's frequent acceleration and deceleration, the IWM's vibration signal is focused. Symptom parameters (SPs) in the time and frequency domains are used to represent different features of the vibration signals in the actual operating conditions of the EV. To select highly sensitive SPs, stable average discrimination rate (SADR) is proposed, which consists of the average discrimination rate (ADR) and the stability coefficient of the group (SCG). Moreover, DBNs are employed to establish a model for the real-time diagnosis of the IWM's mechanical faults, in which the parameter of road-speed-time slice (RSTS) is used to solve the problem that the state transition probability distribution between two continuous time slices cannot be obtained. Finally, the effectiveness of the proposed methods is verified by experiments using the IWM test bench.

INDEX TERMS Dynamic Bayesian networks, electric vehicle, in-wheel motor, real-time diagnosis, road-speed-time slice.

I. INTRODUCTION

Because of environmental pollution caused by conventional fuel vehicles, the development of efficient and environmentally -friendly alternative energy vehicles has been upgraded to the national strategic level [1]–[4]. Due to outstanding advantages such as simple and compact structure and high transmission efficiency, electric vehicles (EVs) powered by multiple in-wheel motors (IWMs) have become a research focus in the field of alternative energy vehicles [5]. IWM technology is one of the core technologies of EVs. However, an IWM is installed in a small hub space, resulting in significant impacts on its performance, such as magnetic field saturation, torque ripple, and load mutation [6], [7]. Furthermore, variable vehicle driving conditions and complex road conditions can lead to mechanical faults in IWMs, resulting in vibration intensification, efficiency reduction, and temperature increase. If an IWM operates long term under mechanical faults, damage such as performance degradation of the insulation material and friction between stator and rotor may occur and cause secondary faults such as wire winding damage, inter-turn circuit, and interphase short circuit faults, which affect driving safety. Therefore, it is necessary to conduct real-time monitoring of the IWM's operating condition and fault diagnosis to improve the accuracy and timeliness of identifying the IWM's faults.

In conventional motors, electrical signals have been used to monitor the motor's operating condition and diagnose some faults. However, the electrical signal of the vehicle power supply is unstable because of the interference resulting from the EV's frequent acceleration and deceleration; therefore, the IWM's vibration signal is focused. Moreover, vibration signals contain abundant state information of the equipment and have the advantages of strong anti-interference ability, as well as the ability to provide information on slight faults [8]–[10]. Methods for monitoring and diagnosing the operating conditions of mechanical equipment based on vibration signals have developed rapidly in recent

The associate editor coordinating the review of this article and approving it for publication was Dong Wang.

years [11]–[15]. In 2014, an intelligent diagnostic method based on the characteristic signals of the best fault frequency region extracted from vibration signals using statistical filtering, support vector machine, possibility theory, and Dempster–Shafer (D-S) evidence theory was proposed to conduct a fault diagnosis of a centrifugal pump system [16]. In 2017, a novel machine learning method called artificial hydrocarbon network was used to extract fault features from vibration signals for the fault diagnosis of sealed deep groove ball bearings [17]. Besides, another intelligent diagnostic system based on the optimal set of feature parameters with a support vector machine was developed to identify different faults in the same year [18]. In 2018, a step-by-step fuzzy diagnostic method based on the symptom parameters (SPs) in the frequency domain was proposed for the diagnosis of structural faults of a rotating machine using trivalent logic fuzzy diagnosis (TLFD) [19]. Moreover, a signal feature extraction and fault diagnosis method based on a statistic filter (SF), the moving-peak-hold method (M-PH), wavelet package transform (WPT), and decision tree was proposed for the fault diagnosis of low-speed rotation machinery [20]–[25]. To some extent, these methods promoted the development of on-line monitoring methods to determine the status of rotating machinery. However, the recognition rate for the operating conditions of IWMs is lower than expected because of the complex running environment of IWMs and the large fluctuation in the vehicle power supply used in EV; therefore, existing methods do not meet the requirements for the safe operation of the vehicle.

Dynamic Bayesian networks (DBNs) combine multiple features related to target types at different moments and represent a tool for the modeling and inferring of dynamic uncertain events; this method thus overcomes the limitations of relying on a single feature [26]–[28], [29]. DBNs have been applied in the area of fault diagnosis in recent years. For example, an innovative approach based on the DBN framework was introduced for the fault detection, identification, and recovery (FDIR) of autonomous spacecraft and the approach was implemented using onboard software architecture in 2014 [30]. In 2016, an electronic equipment health diagnosis system was established based on a three-stage amplifier circuit Bayesian evaluation model of three health states [31]. Also, a fault diagnosis approach using DBNs was proposed to identify the component faults and distinguish the fault types of an electronic system in 2017 [32]. Additionally, a DBN model was developed to obtain the temporal and spatial correlations of intelligent connected vehicles (ICVs) for accurate real-time or historic fault detection and repair in 2018 [33]. In this paper, a new real-time diagnosis method based on DBNs is proposed to determine the mechanical faults of an IWM and the stable average discrimination rate (SADR) is presented to select multiple highly sensitive SPs that are regarded as the IWM's running states as an input to the diagnosis model. In Section II, the IWM test bench is introduced; it simulates the actual operating condition of the IWM in the EV and includes the IWM's installation position, vehicle power supply, road shock, and vertical loads. In Section III, the SADR is defined and the performance of four highly sensitive SPs in the time and frequency domains is described. In Section IV, a Gaussian mixture model (GMM) and different transition probability distributions of two road-speed-time slices (RSTSs) are used to develop a real-time diagnosis model; the model performance is verified using practical experiments under different speed and road conditions.

II. IWM TEST BENCH FOR FAULT DIAGNOSIS

A test bench based on the actual operating conditions of the IWM in an EV was designed, as shown in Fig. 1. The main structure consists of an electric wheel clamp, a shock absorber, an electric wheel (IWM mounted in a housing), a drum roller support, an INSTRON single channel electro-hydraulic servo test system, a pressure sensor, and an acceleration sensor. The acceleration sensor is used to acquire vibration signals of IWM and the placement is shown in Fig. 1. The test data were collected using an LMS multi-function data acquisition instrument with sampling frequency of 12.8 kHz and sampling time of 45 s. In the experiment, the hydraulic vibration platform is raised to contact the roller support frame. When the double rollers on the support frame are in contact with the electric tire surface and the pressure reaches a predetermined value for simulating the vertical load of the vehicle on the electric wheel, the electric wheel starts working. After the speed of the electric wheel reaches a certain value, different levels of the road load spectrum are input to the INSTRON single-channel electro-hydraulic servo test system for simulating the operation of the electric wheel on the road surface. Then three road levels of A, B and C are set for the IWM test. To ensure that the bench test closely approximates a real vehicle test, the power supply system provided by the EV is used to supply electricity and control.

In practical application, there are many mechanical faults of the IWM [34]. In this paper, bearing outer race fault of the IWM is selected as a typical fault, and the fault was artificially made by a wire-cutting machine. The degree of bearing defect was the width of 0.5 mm and the depth of 0.5 mm, as shown in Fig. 2.

In real operation, the vibrations of IWM contain the noises from changing environment such as the disturbance of dynamic load over suspension of the vehicle. Then, an interference source with a frequency of 250 Hz is attached close to the IWM bearing to cause interference vibration signals for simulating the noises.

In the study, the RIICH M1-EV weighing 1060 kg is used as the research prototype. The operation of the test bench is simulated by assuming that the EV is operated by a driver weighing 60 kg on different road levels including levels A, B, and C. The predetermined value of the pressure sensor is 280 kg, which is one-quarter of the total weight of the vehicle and the driver. Moreover, the power supply and inverter of the EV are used to obtain different speeds of the IWM. In the experiment, the normal and abnormal states of the

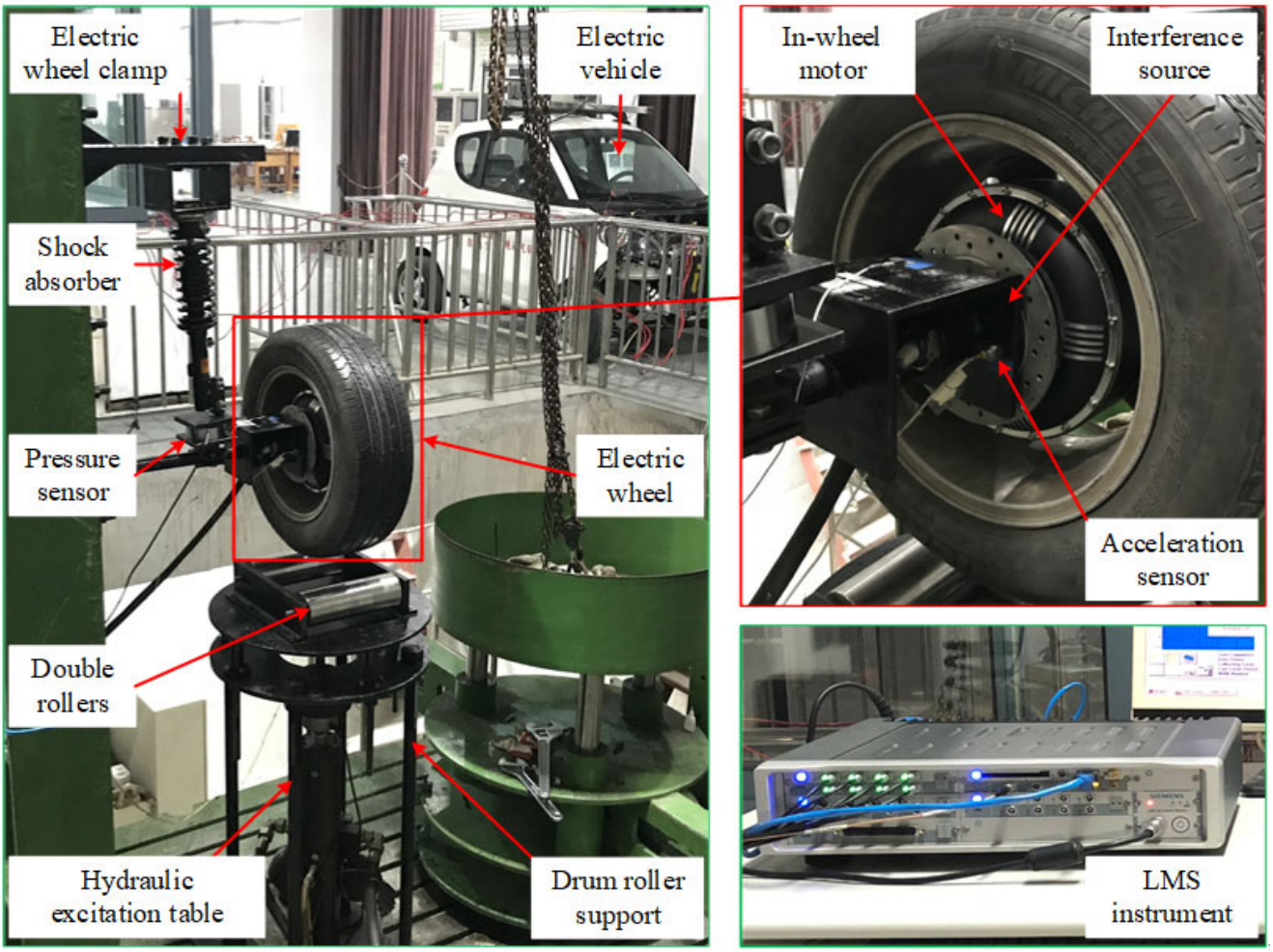

FIGURE 1. IWM test bench.

FIGURE 2. Bearing outer race fault.

IWM at speeds of 10 km/h, 20 km/h, 30 km/h, and 40 km/h were set based on the rotating speed of the IWM. Certainly, the relationship between the vehicle speed and the rotating speed of the IWM is as follows:

$$v = \frac{\pi d \times 3.6n}{60} \tag{1}$$

where v is the vehicle speed. $d = 0.565$m, which is the diameter of the tyre, n is the rotating speed of the IWM, which is inputted artificially. Concretely, the corresponding values of the vehicle speed and the rotating speed of the IWM are shown in Table 1.

TABLE 1. The corresponding values of the vehicle speed and the rotating speed of the IWM.

Rotating speed n (rpm)	Vehicle speed v (km/h)
94	10
188	20
282	30
376	40

III. SELECTION OF HIGHLY SENSITIVE SPs FOR FAULT DIAGNOSIS

The vibration information obtained during the operating period of the IWM represents its operating conditions. Therefore, it is vital to select and extract highly sensitive SPs

from the vibration signals for fault diagnosis and fault-type recognition [35]. However, the mechanical fault features of the IWM are often concealed by the effect of different speeds and different road levels; therefore, it is necessary to conduct a comprehensive analysis of the normal and abnormal states in order to obtain highly sensitive SPs. In this study, the vibration signals are preprocessed using a bandpass filter with 100-2000 Hz to calculate 10 SPs in the time and frequency domains. The SADR method is proposed for the selection of sequentially highly sensitive SPs.

A. SYMPTOM PARAMETERS OF VIBRATION SIGNAL

The time-domain signal is the original basis for fault diagnosis. SPs in the time domain are used to identify different types of faults because there are many parameters for the operating information and they are intuitive and easy to understand. The frequency-domain signal, which is a type of time-domain signal, reflects the changes in the frequency of the mechanical equipment's operating status caused by mechanical faults. Small mechanical faults can be quickly identified by analyzing the composition and amplitude of the frequency components. Therefore, it is necessary to analyze the vibration signals simultaneously in the time and frequency domain [36]–[38]. In this study, 10 SPs are pre-selected in the time and frequency domain, respectively. P_1-P_5 are defined in the time domain and P_6-P_{10} are defined in the frequency domain, as follows.

$$P_1 = \frac{1}{\sigma^4}\sum_{i=1}^{N}(x_i - \bar{x})^4 \tag{2}$$

$$P_2 = \frac{1}{N_p\sigma}\sum_{j=1}^{N_p}\overline{|x_{pj}|} \tag{3}$$

$$P_3 = \sqrt{\frac{1}{N}\sum_{i=1}^{N}x_i^2} \tag{4}$$

$$P_4 = \frac{1}{N_p}\sum_{j=1}^{N_p}\overline{|x_{pj}|} \tag{5}$$

$$P_5 = \left|\frac{1}{\sigma_p^3}\sum_{j=1}^{N_p}(x_{pj} - \overline{x_p})^3\right| \tag{6}$$

where $\{x_i\}$ $(i = 1 - N)$ is the digital data of the vibration signal. N is the number of x_i. $\bar{x}$ is the mean value of $\{x_i\}$, $\bar{x} = \sum_{i=1}^{N} x_i \Big/ N$. σ is the standard deviation of $\{x_i\}$, $\sigma = \sqrt{\sum_{i=1}^{N}(x_i - \bar{x})^2 \Big/ (N-1)}$. $\{x_{pj}\}(j = 1 - N_p)$ is the peak value of $\{x_i\}$. N_p is the number of x_{pj}. $\overline{x_p}$ is the mean value of $\{x_{pj}\}$, $\overline{x_p} = \sum_{j=1}^{N_p} x_{pj} \Big/ N_p$. $\overline{\sigma_p}$ is the standard deviation of $\{x_{pj}\}$, $\sigma_p = \sqrt{\sum_{j=1}^{N_p}(x_{pj} - \overline{x_p}) \Big/ (N_p - 1)}$.

$$P_6 = \frac{1}{\sigma_f^3 I}\sum_{i=1}^{I}(f_i - \bar{f})^3 \cdot F(f_i) \tag{7}$$

$$P_7 = \frac{1}{\sigma_f^4 I}\sum_{i=1}^{I}(f_i - \bar{f})^4 \cdot F(f_i) \tag{8}$$

$$P_8 = \sqrt{\sum_{i=1}^{I} f_i^4 \cdot F(f_i) \Big/ \sum_{i=1}^{I} f_i^2 \cdot F(f_i)} \tag{9}$$

$$P_9 = \sum_{i=1}^{I} F(f_i) \tag{10}$$

$$P_{10} = \sqrt{\sum_{i=1}^{I} F^2(f_i)} \tag{11}$$

where $\{f_i\}$ $(i = 1 - I)$ is the frequency sequence. I is the number of half of the sampling frequency. $F(f_i)$ is the spectrum value of f_i. $\bar{f}$ is the average frequency, $\bar{f} = (\sum_{i=1}^{I} f_i \cdot F(f_i)) \Big/ \sum_{i=1}^{I} F(f_i)$. σ_f is the standard variance, $\sigma_f = \sqrt{\frac{1}{I}\sum_{i=1}^{I}(f_i - \bar{f})^2 \cdot F(f_i)}$.

B. SELECTION OF HIGHLY SENSITIVE SPs

The sensitivity of the SPs reflects the ability of the SPs to distinguish among different operating states of the equipment. The sensitivities of different SPs are different even if the mechanical equipment is in the same operating state. In addition, the sensitivity of the same SP is different when the mechanical equipment operates in different states. However, the more sensitive the SPs are, the easier it is to distinguish between normal and fault states. Otherwise, it is difficult to distinguish between different states if the sensitivity of the SPs is low. In order to select highly sensitive SPs, many methods have been proposed such as the Principal Component Analysis (PCA) and the distinguish index (DI) [39], [40]. The idea of PCA is to map n-dimensional features to k-dimensional (k < n), which is a completely new orthogonal feature. This k-dimensional feature is called principal component. Considering this, PCA is a good way to select SPs. However, due to the complex driving conditions of vehicles, the model that reduce from n-dimensional space to k-dimensional space cannot be determined only. So the timeliness of the PCA method is poor, which cannot meet the requirement of the real-time diagnosis. Besides, the DI-based method has been widely applied. The DI is defined by the following equation:

$$DI = \frac{|\mu_2 - \mu_1|}{\sqrt{\sigma_1^2 + \sigma_2^2}} \tag{12}$$

where μ_1, μ_2 represent the average value of state 1 and state 2 of an SP and σ_1, σ_2 represent the corresponding standard deviations, respectively. The discrimination rate (DR), which is the ability of an SP to distinguish between two states, is defined by (12) and is based on the DI value. The relationship among the DI value, the DR value and the sensitivity of a SP is shown in Table 2 [41]. It is apparent that the larger the value of the DI, the larger the value of the DR is, therefore, the more sensitive the SP is.

$$DR = 1 - \frac{1}{\sqrt{2\pi}} \int_{-\infty}^{-DI} e^{-\frac{x^2}{2}} dx \tag{13}$$

TABLE 2. The relationship among DI, DR and sensitivity of a SP.

DI	DR	SP's Sensitivity
<0.85	<80%	low
0.85-1.30	80%-90%	slightly low
1.30-1.65	90%-95%	medium
1.65-2.33	95%-99%	high
>2.33	>99%	very high

When using the DI-based method, it is very effective and quick to select only one SP for distinguishing between two states. However, the operating conditions of mechanical equipment are complex and changeable and many faults with different degrees can occur under any condition; therefore, a single SP cannot provide sufficient information on the vibration signal. Misdiagnosis may occur if one relies on only one parameter. Therefore, multiple highly sensitive SPs need to be selected concurrently for a more accurate diagnosis but the performance of the DI-based method is unsatisfactory for this purpose. In order to select multiple highly sensitive SPs at the same time, a new method is proposed in this study; it uses a parameter called the SADR, which consists of the average discrimination rate (ADR) and the stability coefficient of the group (SCG) based on the DR. Multiple highly sensitive SPs can be selected in the following two steps using this method.

Step 1: Preliminary selection based on the ADR. The ADR is defined as follows:

$$ADR = \frac{1}{R \cdot V \cdot G} \sum_{r=1}^{R} \sum_{v=1}^{V} \sum_{g=1}^{G} DR_{rvg} \tag{14}$$

where R is the number of different road levels. V is the number of different speeds. G is the number of fault types. In this study, three road levels, four speeds, and a typical fault are considered so that R, V, and G are 3, 4, and 1, respectively. For the description, specific symbol with the information of road type and speed level is used to express each IWM operating state, as shown in Table 3. DR of each IWM operating state is shown in Fig. 3. The ADR values of the 10 SPs are shown in Table 4.

TABLE 3. Corresponding relation of specific symbol and each IWM operating state.

Road level	Speed level (km/h)			
	10	20	30	40
A	A10	A20	A30	A40
B	B10	B20	B30	B40
C	C10	C20	C30	C40

If the DR of an SP is 95%, the SP is highly sensitive to the two operating states, as shown in Table 2. The same applies to the ADR. That is to say, if the ADR of an SP is 95%, the SP is highly sensitive to multiple operating states. Therefore, the SPs in the preliminary selection are P_3, P_4, P_6, P_7, P_8, P_9, and P_{10}. However, it is crucial to maintain a balance between the time domain and frequency domain when selecting the SPs for better results. In this study, four highly sensitive SPs

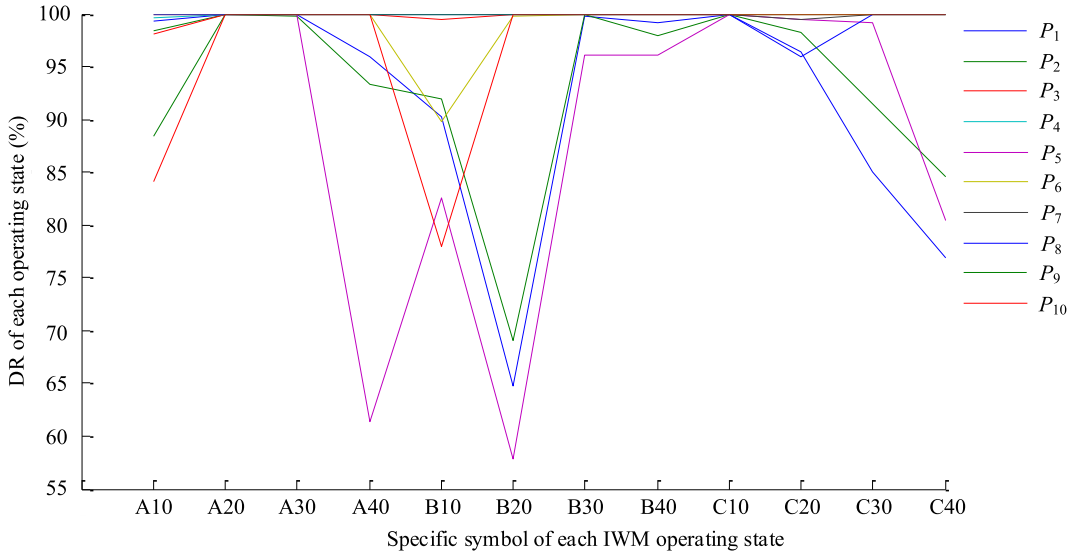

FIGURE 3. DR of each IWM operating state.

TABLE 4. ADR values of the 10 SPs.

Road level	Speed level (km/h)	DR of each SP (%)									
		P_1	P_2	P_3	P_4	P_5	P_6	P_7	P_8	P_9	P_{10}
A	10	99.24	98.45	98.09	99.66	99.99	99.99	99.99	100	88.46	84.25
A	20	99.99	99.99	100	100	99.99	100	100	100	99.99	99.87
…	…	…	…	…	…	…	…	…	…	…	…
C	40	76.91	84.54	100	99.99	80.38	99.99	100	100	100	100
ADR of each SP (%)		92.28	93.71	99.79	99.97	93.71	99.12	99.96	99.66	99.02	96.82

are required, which means that two SPs are selected in the time domain and two are selected in the frequency domain. It is evident that the highly sensitive SPs in the time domain are P_3 and P_4 in the preliminary selection. The problem is the selection of highly sensitive SPs in the frequency domain; therefore, a secondary selection is performed in step 2.

Step 2: Secondary selection based on the SCG

The stability of the SP to identify faults in different operating states can be assessed through the standard deviation of the DR of the SP. The smaller the value of the standard deviation, the more stable the SP is. Therefore, the SCG is proposed to assess the stability of the whole group; it consists of the standard deviations of the selected SPs. The SCG is defined as follows:

$$SCG = \sum_{q=1}^{Q} \sqrt{\frac{1}{H-1} \sum_{h=1}^{H} (DR_{hq} - ADR_q)^2} \qquad (15)$$

where Q is the number of the required highly sensitive SPs. H is the number of the operating states and equals $R \cdot V \cdot G$ in step 1. Therefore, Q and H are 2 and 12 respectively in the subsequent selection of highly sensitive SPs in the frequency domain. The SCG values of the different groups with the two SPs are shown in Table 5.

TABLE 5. SCG values of different groups with two SPs.

Group number	SPs	SCG	ADRmax(%)	ADRmin(%)
1	P_6, P_7	0.0307	99.96	99.12
2	P_6, P_8	0.0624	99.66	99.02
…	…	…	…	…
5	P_7, P_8	0.0133	99.96	99.66
…	…	…	…	…
10	P_9, P_{10}	0.1507	99.02	96.82

The value of the SCG of the 5th group is the minimum value and the selected highly sensitive SPs are P_7 and P_8 in the frequency domain. Therefore, P_3, P_4, P_7, and P_8 are confirmed as the diagnostic SPs.

IV. REAL-TIME DIAGNOSIS OF THE MECHANICAL FAULTS OF THE IWM BASED ON DBNS

The diagnosis of the mechanical faults of the IWM is a dynamic process in an actual operation. Since the operating conditions vary continuously and there are many interference factors, it is important to use a parameter to determine whether the IWM's operating condition is normal or not. DBNs are used to obtain dynamic probability inference [42], [43]. This is achieved by the DBNs' initial network and transfer network. Since the SPs are continuous and follow a Gaussian distribution, a GMM is used to develop the real-time diagnostic model of the mechanical faults of the IWM.

A. DYNAMIC BAYESIAN NETWORKS BASED ON A MIXTURE OF GAUSSIAN OUTPUTS

DBNs usually consist of a limited number of time slices (TSs), each of which consists of a directed acyclic graph (DAG) and conditional probability tables (CPT) [44]. The transition probability distribution $P(C^t|C^{t-1})$ between two TSs and the probability distribution of the observable variables $P(X^t|C^t)$ [45] are required when DBNs are used to for the identification and diagnosis of operating states. Gaussian mixture output dynamic Bayesian networks (GMODBNs) can be developed based on a GMM, which is a special type of DBN, in which the probability distribution of the observable variables is represented by a Gaussian mixture [46]. The GMODBNs in two TSs are shown in Fig. 4.

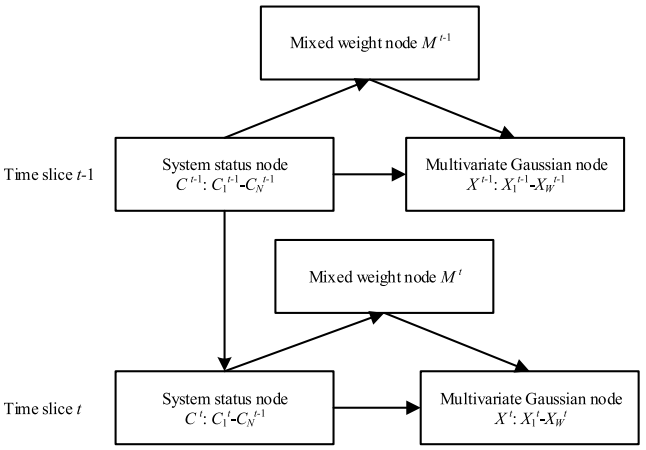

FIGURE 4. GMODBNs in two time slices.

In the t^{th} TS, the parent node C^t contains the information of N operating states of the system, C_1^t, C_2^t, …, C_N^t. The mixed weight node Mt contains the information of K mixed components of the mixed model. The mixed weights m_1^t, m_2^t, …, m_K^t are reflected by the CPTs of node M^t. The child node X^t

is a multivariate Gaussian node containing the observable information of W features, $X_1^t, X_2^t, \ldots, X_W^t$.

In the t-1$^{\text{th}}$ TS, the system status node is represented as $C_i^{t-1}(1 \le i \le N)$ while in the TS t, the system status node is represented as $C_j^t(1 \le j \le N)$ and the observable feature node is represented as X^t including all the features $X_1^t, X_2^t, \ldots, X_W^t$. Then, the probability distribution of observable variables can be obtained with the following equation:

$$P(X^t|C_j^t) = \sum_{k=1}^{K} P(X^t|M_k^t, C_j^t)P(M_k^t|C_j^t) \tag{16}$$

The posterior probability of the system status node in the TS t can be calculated by the following equation based on the Bayesian formula [47].

$$P(C_j^t|X^t, C_i^{t-1}) = \frac{P(X^t|C_j^t)P(C_j^t|C_i^{t-1})}{\sum_{n=1}^{N} P(X^t|C_n^t)P(C_n^t|C_i^{t-1})} \tag{17}$$

The conditional probability distribution $P(M_k^t|C_j^t)$ of the mixed components, the Gaussian mixture conditional probability distribution $P(X^t|M_k^t, C_j^t)$, and the transition probability distribution $P(C_t|C_{t-1})$ can be obtained by Bayesian parameter learning methods based on the sample data or expert knowledge [48].

B. THE DIAGNOSITIC MODEL OF THE IWM AND THE REAL- TIME DIAGNOSTIC METHOD

Traditional DBNs are unrolled in limited TSs and the transition probability distribution is the link between two adjacent TSs [49], [50]. However, there is no iron link between the operating state of the IWM in the previous TS and the operating state in the current TS because of variable speed and uncertain road levels, i.e., the transition probability distribution between the two adjacent TSs is impossible to obtain. When the EV driven by the IWM operates on the road, a sudden speed increase and higher road level will increase the vehicle turbulence, thereby increasing the change in the dynamic load and impact on the IWM bearing so that local deformation of the IWM bearing can easily occur and lead to mechanical faults [51]. If the vehicle operates on a lower road level at lower speed, there is still a certain probability of failure in spite of the reduced impact on the IWM bearing. Therefore, the changes in the IWM operating state can be described as a series of snapshots that change with the vehicle speed and road levels. Each snapshot obtains the information of the IWM's operating state at a specific speed on a specific road level in a specific TS. This snapshot is referred to as the RSTS.

Fig. 5 is the transformation process from TS to RSTS. Here, a cuboid is used to express the multi-dimensional spaces of the vibration-based SPs at some road level and speed level. For detailedly introducing the transformation from TS to RSTS, the state vectors of speed s^i, load condition r^i and vibration v^i in the i^{th} snapshot are

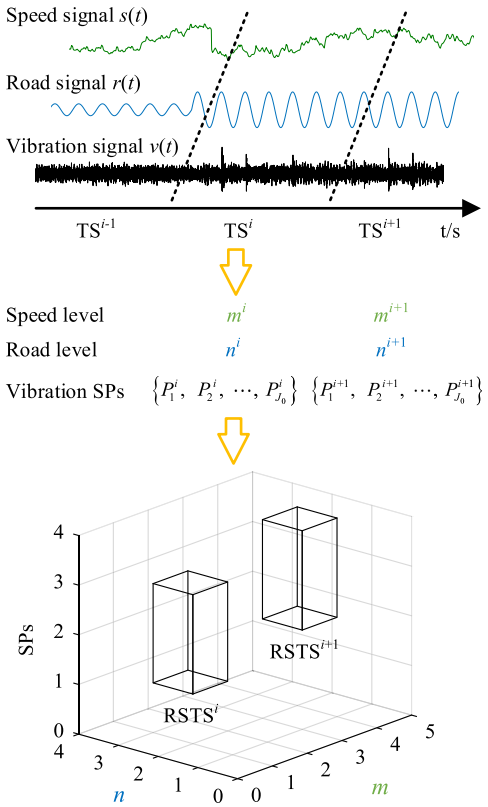

FIGURE 5. Transformation process from TS to RSTS.

given as

$$s^i = \left[s_{(i-1)\Delta t+1},\ s_{(i-1)t+2},\ \cdots s_{i\cdot\Delta t} \right] \tag{18}$$

$$r^i = \left[r_{(i-1)\Delta t+1},\ r_{(i-1)t+2},\ \cdots r_{i\cdot\Delta t} \right] \tag{19}$$

$$v^i = \left[v_{(i-1)\Delta t+1},\ v_{(i-1)t+2},\ \cdots v_{i\cdot\Delta t} \right] \tag{20}$$

where s_i, r_i and v_i are the i^{th} sampling point in time-series signals of speed $s(t)$, load condition $r(t)$ and vibration $v(t)$, respectively. Δt is time interval of each snapshot. Then the information set of the i^{th} TS can be expressed as

$$\text{TS}^i = \left\{ s^i,\ r^i,\ v^i \right\} \tag{21}$$

Since s^i, r^i and v^i flow through time, and the actual operating state of IWM is fickle, TS^i is a transient vector. In order to weaken the timeliness of TS^i, s^i, r^i and v^i are analyzed to extract the features. The average values $\bar{s}^i$ and $\bar{r}^i$ are used to express the features of s^i and r^i, respectively. Some highly sensitive SPs $P_j^i (j = 1, 2 \ldots J_0)$ selected by SADR are used to represent the vibration v^i, and J_0 is the number of the selected SPs. Then TS^i can be abstracted as

$$\text{TS}^i = \left\{ \bar{s}^i,\ \bar{r}^i,\ P_1^i, P_2^i, \cdots, P_{J_0}^i \right\} \tag{22}$$

However, the IWM's speed and load condition vary constantly, $\bar{s}^i$ and $\bar{r}^i$ are still continuous variables. The class-dependent discretization [52] and the road model parameters of road level evaluation are borrowed to disperse $\bar{s}$ and $\bar{r}$ for

multiple discrete intervals, as follows

$$\hat{s} = \{m \,|\bar{s} \in [10 \cdot m - 5,\ 10 \cdot m + 5)\} \tag{23}$$

$$\hat{r} = \{n \,|\rho_{\bar{r}} \in [37.5 \cdot (n-1),\ 37.5 \cdot n)\} \tag{24}$$

where $\rho_{\bar{r}}$ is the standard deviation of vertical vibrational acceleration. $\hat{s}$ is speed level. If the speed fluctuates in the range of 5 km/h above and below the fixed value, the fixed value shall be regarded as the speed level. Especially, when the vehicle speed is lower than 5 km/h, which means the IWM runs in a low speed state, the speed level is considered as 0 since the characteristic signal is not obvious. In general, the maximum value of m is 12. $\hat{r}$ is road level that is divided into A, B, C and D. Here, the numbers 1, 2, 3 and 4 are used to denote road level, and the smaller the value, the higher the load level. Then TS^i with discretization and digitization is shown as

$$\mathrm{TS}^i = \left\{ m^i,\ n^i,\ P_1^i, P_2^i, \cdots, P_{J_0}^i \right\} \tag{25}$$

In order to weaken the timeliness of TS, speed level m and load level n are regarded as independent variables, and some SPs of vibration information are considered as dependent variables, then three-dimensional RSTS is reconstructed as

$$\mathrm{RSTS}^i = \left\{ (P_1, P_2, \cdots, P_{J_0})^i_{k_1,k_2} \,|k_1 \in M, k_2 \in N \right\} \tag{26}$$

where M and N are the sets of independent variables m and n, respectively. $(P_1, P_2, \cdots, P_{J_0})$ is the array of all selected SPs.

For three-dimensional RSTS, the variables of speed level and load level are given priority. The first consideration of two adjacent RSTSs is whether they are in the condition with the same speed level and load level. If so, the transition probability distribution is obtained by expert knowledge [53] on the basis of the experimental data from the IWM test. If not, expert knowledge is only considered to construct the DBNs in the process of determining the transition probability distribution. In the study, the IWM test with 4 speed levels and 3 load levels has been performed, and P_3, P_4, P_7, and P_8 are confirmed as the diagnostic SPs. Moreover, the length of a TS is 3 s. The signal of vehicle speed is obtained from the controller area network (CAN) of the vehicle communication system, and the road level is identified based on the vertical vibrational acceleration from the acceleration sensor by the method proposed in reference [54]. Then the IWM mechanical fault diagnosis model has been created based on the DBNs in the same condition. Fig. 6 shows the unrolled mechanical fault diagnostic model of the IWM in two RSTSs.

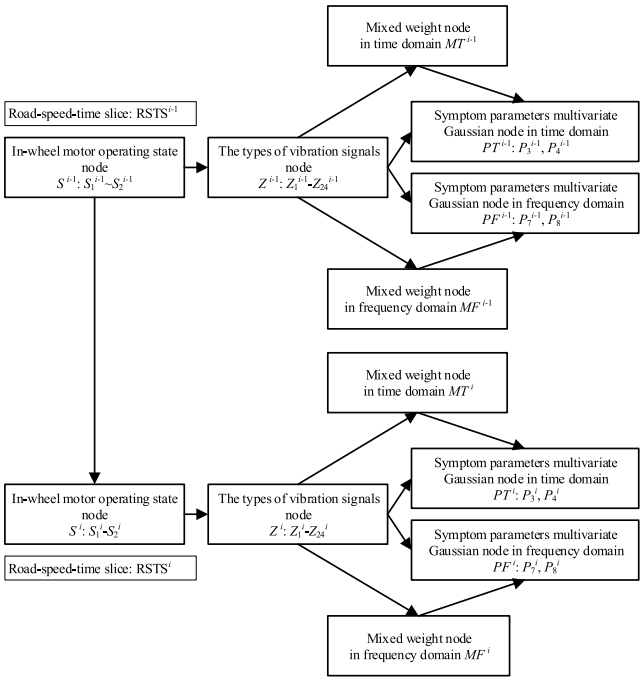

FIGURE 6. Unrolled mechanical fault diagnosis model of the IWM in two RSTSs.

In the i^{th} RSTS^i, S^i represents the IWM's operating state node. S_1^i represents the normal operating state and S_2^i represents the fault operating state. Z^i is the node containing the information of 24 types of vibration signals. The corresponding road level, speed level, and operating state (normal or fault) of Z_1^i-Z_{24}^i are shown in Table 6. MT^i is the mixed weight node in the time domain and each vibration signal to be diagnosed is considered to be composed of 24 mixed components in the time domain. MF^i is the mixed weight node in the frequency domain and each vibration signal to be diagnosed is considered to be composed of 24 mixed components in the frequency domain. PT^i is the multivariate Gaussian node of the highly sensitive SPs including P_3^i and P_4^i in the time domain. PF^i is the multivariate Gaussian node of the highly sensitive SPs including P_7^i and P_8^i in the frequency domain. PT^i and PF^i are the observed nodes of the model.

The CPT of each node is obtained by parameter learning and the transition probability distributions between the two adjacent RSTSs are obtained by expert knowledge; the results are shown in Table 7. Subsequently, the group of mechanical fault diagnosis models of the IWM in the two RSTSs is developed based on the conditional probability distribution of

TABLE 6. The corresponding road level, speed level, and operating state of Z_1^i-Z_{24}^i.

Road level	A				B				C			
Speed level (km/h)	10	20	30	40	10	20	30	40	10	20	30	40
Normal	Z_1^i	Z_2^i	Z_3^i	Z_4^i	Z_5^i	Z_6^i	Z_7^i	Z_8^i	Z_9^i	Z_{10}^i	Z_{11}^i	Z_{12}^i
Fault	Z_{13}^i	Z_{14}^i	Z_{15}^i	Z_{16}^i	Z_{17}^i	Z_{18}^i	Z_{19}^i	Z_{20}^i	Z_{21}^i	Z_{22}^i	Z_{23}^i	Z_{24}^i

TABLE 7. State transition probability distribution between two continuous RSTS in the IWM's diagnostic model.

$RSTS^{i-1}$ with different speed levels and road levels			$RSTS^{i}$ with different speed levels and road levels								
			A road level				…	C road level			
Road level	Speed level (km/h)	State	10km/h		20km/h		…	30km/h		40km/h	
			Normal	Fault	Normal	Fault	…	Normal	Fault	Normal	Fault
A	10	Normal	0.99	0.01	0.98	0.02	…	0.92	0.08	0.88	0.12
		Fault	0	1	0	1	…	0	1	0	1
	20	Normal	0.99	0.01	0.99	0.01	…	0.96	0.04	0.94	0.06
		Fault	0	1	0	1	…	0	1	0	1
…	…	…	…	…	…	…	…	…	…	…	…
C	30	Normal	0.99	0.01	0.99	0.01	…	0.99	0.01	0.96	0.04
		Fault	0	1	0	1	…	0	1	0	1
	40	Normal	0.99	0.01	0.99	0.01	…	0.99	0.01	0.98	0.02
		Fault	0	1	0	1	…	0	1	0	1

the nodes in a single RSTS and different transition probability distributions. The Bayesian network of a single RSTS is the same and the only difference between the diagnostic models is the transition probability distribution.

With the establishment of IWM's fault diagnosis models in any two RSTSs, real-time diagnosis system is built to achieve real-time diagnosis and monitoring of the IWM's operating states, as shown in Fig. 7.

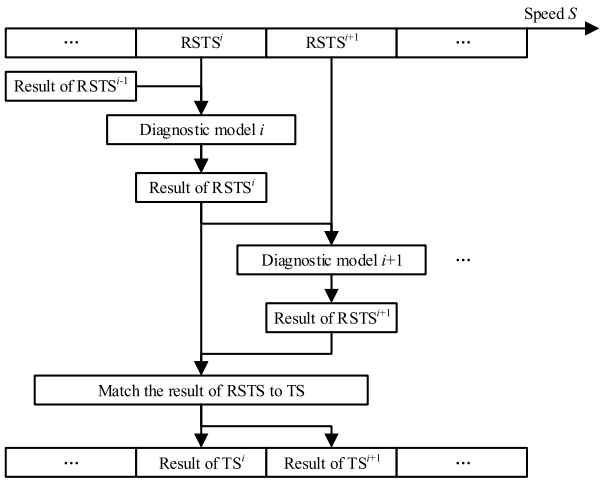

FIGURE 7. Real-time diagnosis system for IWM.

Firstly, TS^i in current state is transformed to $RSTS^i$ according to the previous method, and the speed levels and load levels between $RSTS^{i-1}$ and $RSTS^i$ are examined to select the corresponding diagnosis model i. Secondly, the array of the selected SPs in $RSTS^i$ and the result of $RSTS^{i-1}$ are input into the diagnosis model i for diagnosing the current state. Finally, the diagnosis result of $RSTS^i$ is output as the diagnosis result of TS^i, and is input into the diagnosis model $i+1$ as the previous diagnosis result, and so on, the IWM's operating states is monitored real-timely. Certainly, in real-time diagnostic system, the first RSTS's result is obtained on basis of the Bayesian network of the single RSTS. The operating state of the second RSTS is obtained by combining the result of the first RSTS and the diagnostic model selected from the diagnostic system. For the other continuous RSTSs, the previous RSTS's result is the state input of the latter RSTS. Each RSTS corresponds to only one TS so that the result of each RSTS can be matched to the related TS. Eventually, the IWM's operating state in each TS is judged in the real-time diagnostic system.

For ensuring the robustness of the real-time diagnostic system, a rule has been set that the final diagnostic result of the IWM's operating state is determined only when considering the results in three consecutive TSs synthetically.

C. DIAGNOSIS AND VERIFICATION

To verify the proposed methods, each type of experiment has been repeated 15 times in the same state such as the same control speed and load level, and the length of each TS is set as 3 s. Then each set of experiment data has 15 TSs. Moreover, according to the classification standards of speed level and road level, the normal and abnormal states of the IWM are combined to obtain 24 types of experimental data. Firstly, the experimental data have been divided into 15 portions, and each portion is a TS. Secondly, vibration, road and speed signals of each TS in each state have been processed into highly sensitive SPs of P_3, P_4, P_7, and P_8, road level, speed level, and to transform into RSTS. Finally, the first 13 samples of each type of experiment have been selected to build the training data, and the remaining 2 samples have been used to compose the test data. Fig. 8 is the schematic diagram of experimental signals, training data and test data. Fig. 9 shows the spatial distributions of P_3, P_4, P_7, P_8 between normal state and fault state from the first training data. Here, rhombus and roundness are used to express normal state and fault state, respectively. Each state has 15 RSTSs. P_3, P_4, and P_7 correspond, respectively, to three directions in a three-dimensional diagram. The values of P_8 are expressed by the color depth.

For establishing a uniform standard of diagnosis system, the normal and fault states of the IWM are labeled with 1 and 2, respectively. When the training data with the corresponding labels are input into IWM's diagnosis system altogether, the information of road level and speed level is invoked firstly, the training data with the same conditions are

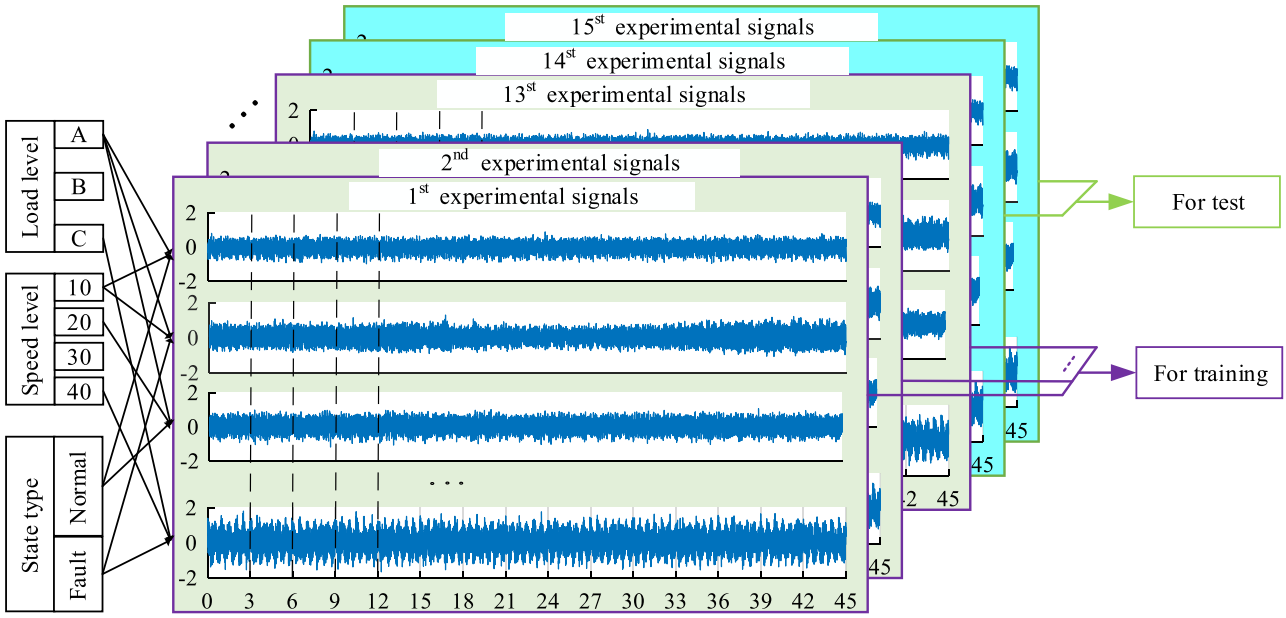

FIGURE 8. The schematic diagram of experimental signals, training data, and test data.

TABLE 8. Test samples with different time slices, speeds levels, road levels, and operating conditions of the IWM.

Sample number	Different condition	1st time slice	2nd time slice	3rd time slice	4th time slice
		10 km/h	20 km/h	30 km/h	40 km/h
Test sample 1	Road level	A	A	A	A
	State	Normal	Normal	Normal	Normal
Test sample 2	Road level	A	A	A	A
	State	Normal	Normal	Normal	Fault
Test sample 3	Road level	A	A	A	A
	State	Fault	Fault	Fault	Fault
Test sample 4	Road level	B	B	B	B
	State	Normal	Normal	Normal	Fault
Test sample 5	Road level	B	B	B	B
	State	Normal	Normal	Fault	Fault
Test sample 6	Road level	B	B	B	B
	State	Fault	Fault	Fault	Fault
Test sample 7	Road level	C	C	C	C
	State	Normal	Normal	Normal	Fault
Test sample 8	Road level	C	C	C	C
	State	Normal	Normal	Fault	Fault
Test sample 9	Road level	C	C	C	C
	State	Fault	Fault	Fault	Fault
Test sample 10	Road level	A	B	C	C
	State	Normal	Normal	Normal	Fault
Test sample 11	Road level	A	B	C	C
	State·	Normal	Normal	Fault	Fault
Test sample 12	Road level	A	B	C	C
	State	Fault	Fault	Fault	Fault

grouped together to train the corresponding diagnostic model. When 24 diagnostic models have been trained successively, the diagnosis system has been established.

Then 24 types of the test data is processed into RSTSs, then these RSTSs are input the diagnosis system one by one for simulating the process of real-time diagnosis. For introducing the performance of the diagnosis system, 4 TSs of 12 types of test samples are shown in Table 8. Certainly, speed levels and road levels in Table 8 are the results processed by Formula (23) and (24), and even if speed levels and road levels are same, there are large differences in the actual operating conditions. Then the corresponding vibration information such as P_3, P_4, P_7, and P_8 has large differences, as shown in Fig. 10. Obviously, the features of 4 TSs are that speed level escalates and road level gradually worsen. Certainly, other 12 types of test samples are not shown, but the features are opposite that speed level degrades and road level gradually ameliorate.

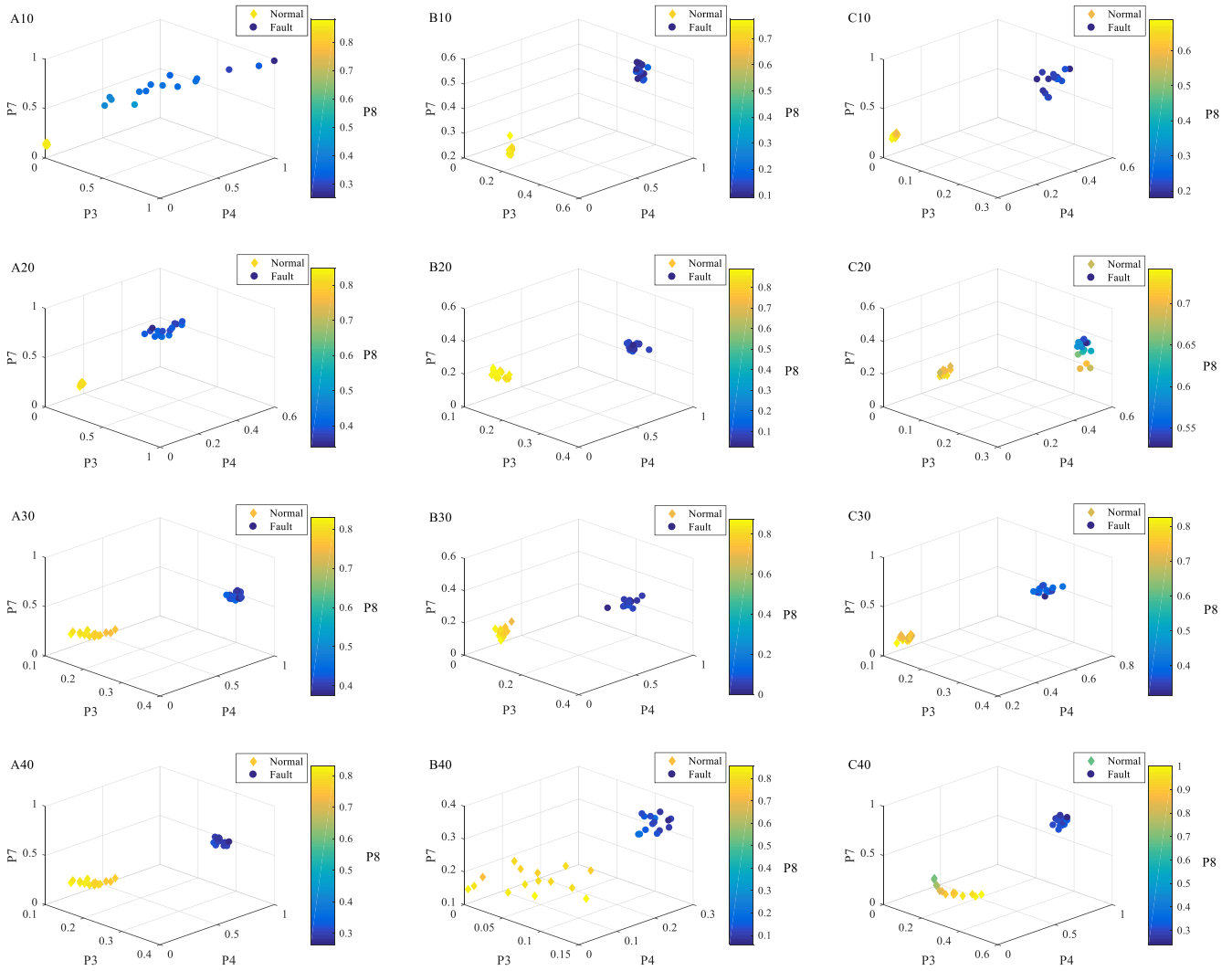

FIGURE 9. The spatial distributions of P_3, P_4, P_7, P_8 between normal state and fault state from the first training data.

TABLE 9. Recognition rate of the mechanical fault diagnosis of the IWM.

Sample number	Recognition rate of different states (S)							
	1st time slice		2nd time slice		3rd time slice		4th time slice	
	S_1	S_2	S_1	S_2	S_1	S_2	S_1	S_2
1	99.99%	0.01%	99.99%	0.01%	99.99%	0.01%	99.98%	0.02%
2	99.99%	0.01%	99.99%	0.01%	99.96%	0.04%	0.01%	99.99%
3	0	100%	0	100%	0.01%	99.99%	0	100%
4	99.99%	0.01%	99.99%	0.01%	99.99%	0.01%	0.01%	99.99%
5	99.99%	0.01%	99.99%	0.01%	0.01%	99.99%	0	100%
6	0.01%	99.99%	0	100%	0	100%	0	100%
7	99.99%	0.01%	99.99%	0.01%	99.99%	0.01%	0.01%	99.99%
8	99.99%	0.01%	99.99%	0.01%	99.99%	0.01%	0	100%
9	0.01%	99.99%	0.01%	99.99%	0.01%	99.99%	0	100%
10	99.99%	0.01%	99.99%	0.01%	99.99%	0.01%	0.01%	99.99%
11	99.99%	0.01%	99.99%	0.01%	99.99%	0.01%	0.01%	99.99%
12	0	100%	0	100%	0	100%	0	100%

When the 1st RSTS of each test sample is input, single RSTS is used to recognize the probability of each state. Here, S_1 and S_2 represent the normal and fault states of the IWM, respectively, and the labels are saved in the diagnosis system. If the probability of S_1 is bigger, the corresponding state of TS is normal; otherwise, the state is abnormal. Then the

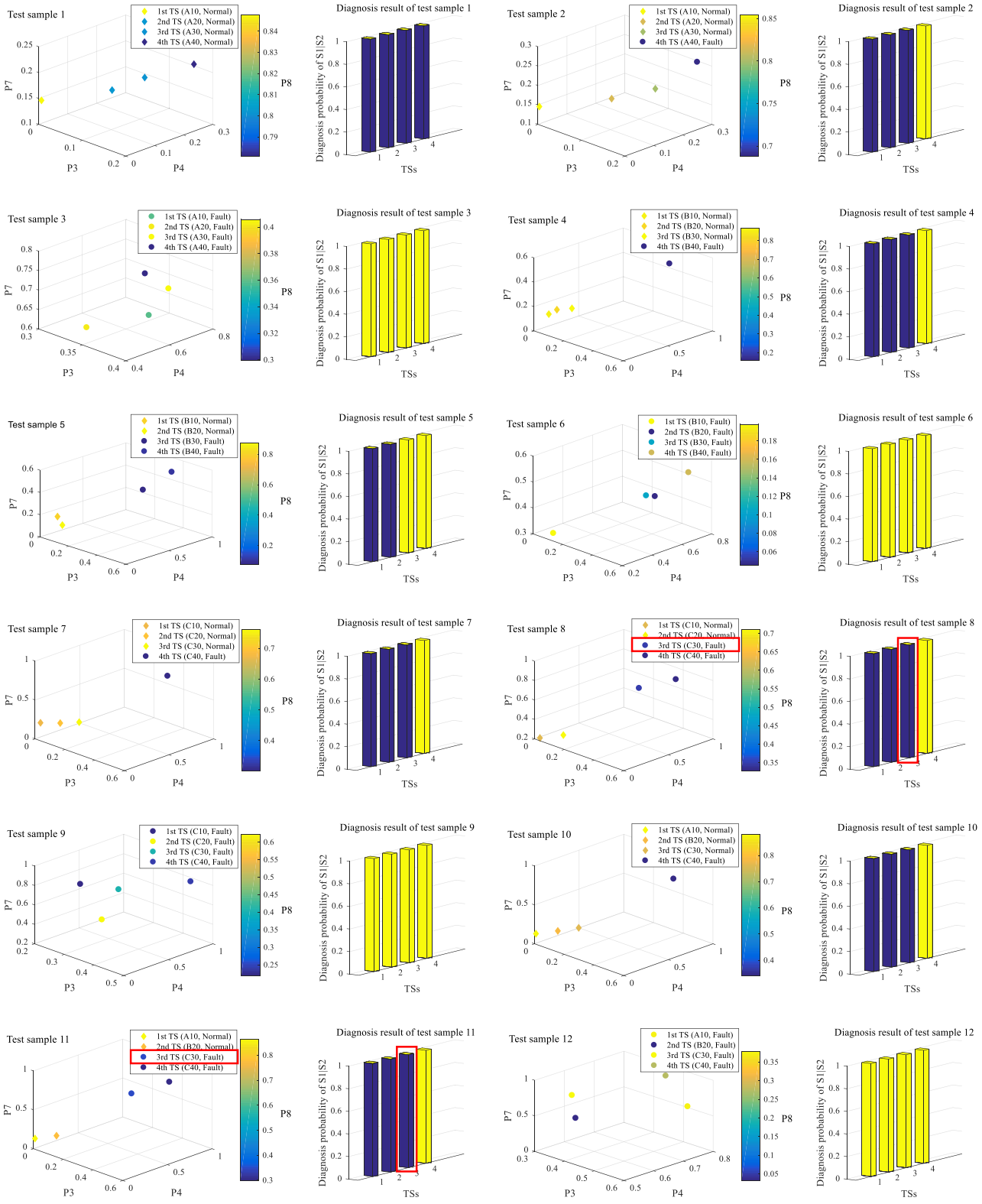

FIGURE 10. 12 types of test samples and the corresponding diagnosis results.

corresponding states of the 3rd, 6th, 9th, and 12th test samples are judged to be abnormal, and other states are normal. These diagnosis results and the initial states are in good agreement.

When the 2nd RSTS of each test sample is input, the corresponding RSTS and the 1st diagnosis result are considered together to decide the probability. And so on, the information

TABLE 10. List of all abbreviations in the paper.

Full name	Abbreviation
in-wheel motor	IWM
electric vehicle	EV
dynamic Bayesian networks	DBNs
Dempster–Shafer	D-S
trivalent logic fuzzy diagnosis	TLFD
moving-peak-hold	M-PH
wavelet package transform	WPT
intelligent connected vehicles	ICVs
symptom parameters	SPs
stable average discrimination rate	SADR
average discrimination rate	ADR
stability coefficient of the group	SCG
Principal Component Analysis	PCA
distinguish index	DI
discrimination rate	DR
directed acyclic graph	DAG
conditional probability tables	CPT
time slice	TS
road-speed-time slice	RSTS
Gaussian mixture model	GMM
Gaussian mixture output dynamic Bayesian networks	GMODBNs

of $RSTS^i$ and the i-1^{th} ($i > 1$) diagnosis result are used to confirm the probability of the i^{th} state. The diagnostic results with the corresponding test samples as shown in Table 8 are shown in Fig. 10, the diagnostic probabilities are listed in Table 9. Comparing the original state of each test RSTS, two of the diagnosis results are inconsistent, as shown in Fig. 10 with red box.

In order to analyze the recognition rate of test TSs, the diagnosis results of other 672 TSs are checked one by one, the states of 28 TSs are only misjudged. Therefore, for single TS, the recognition rate is 95.8%. Moreover, all erroneous judgement TSs with the front and back TSs are synthetically analyzed to find that most of these TSs are in the early stage of IWM fault, and the cases of multiple consecutive TSs misjudged are fewer. There are 7 cases that two consecutive TSs are misjudged, and there are 2 cases that three consecutive TSs are misjudged, while other cases are single TS is misjudged. According to the rule for ensuring the robustness of the real-time diagnostic system, there are 2 times that the system results are incorrect, and the accuracy of the real-time diagnostic system is 99.7%.

V. CONCLUSION

Highly sensitive SPs were selected intelligently by using the SADR to represent the features of the vibration signal in the IWM for different road levels and vehicle speeds. The signal features were extracted under the condition of multiple interference factors. The proposed method is especially applicable to the field of intelligent diagnosis and real-time monitoring.

TSs of DBNs were applied flexibly to determine the RSTSs, which contain additional information on the road level and speed, to develop the RSTS-based diagnostic model. The method effectively deals with the problem that the transition probability distribution between two adjacent TSs cannot be obtained and promotes the development and application of diagnostic techniques in a complex and variable operating environment.

A real-time diagnostic method was proposed by targeting the IWM's mechanical faults. The practical experiments performed using the IWM test bench verified the effectiveness of the proposed method. The diagnostic results showed that the recognition rate of the mechanical faults of the IWM was 95.8% for single TS, and was 99.7% for the real-time diagnostic system. Because of the complexity and variability of vehicle driving conditions, the current research focuses on whether the fault state can be identified. In the future, the early fault of IWMs will be deeply studied. Moreover, the distributed drive system of an EV will be focalized, which usually includes even a number of IWMs, to investigate the effective monitoring of the real operating conditions and diagnose system faults.

APPENDIX

See Table 10.

REFERENCES

[1] T. Stock and G. Seliger, "Opportunities of sustainable manufacturing in industry 4.0," *Procedia CIRP*, vol. 40, pp. 536–541, Aug. 2016.

[2] T. D. Oesterreich and F. Teuteberg, "Understanding the implications of digitisation and automation in the context of Industry 4.0: A triangulation approach and elements of a research agenda for the construction industry," *Comput. Ind.*, vol. 83, pp. 121–139, Dec. 2016.

[3] E. Hofmann and M. Rüsch, "Industry 4.0 and the current status as well as future prospects on logistics," *Comput. Ind.*, vol. 89, pp. 23–34, Aug. 2017.
[4] Y. Lu, "Industry 4.0: A survey on technologies, applications and open research issues," *J. Ind. Inf. Integr.*, vol. 6, pp. 1–10, Jun. 2017.
[5] Q. H. Ming and K. C. Xu, "Analysis of in-wheel motor system and drive technology," *Shanghai Auto*, vol. 3, pp. 6–7, Jul. 2017.
[6] Y. Li, X. Xu, and X. D. Sun, "Review and future development of in-wheel motor drive technology," *Electr. Mach. Control Appl.*, vol. 44, pp. 1–7, Jul. 2017.
[7] R. He and R. J. Zhang, "Research and development of in-wheel motor drive technology," *J. Chongqing Univ. Technol. (Natural Sci.)*, vol. 29, no. 17, pp. 10–18, 2015.
[8] H. T. Xue, Z. X. Li, Y. Li, H. Jiang, and P. Chen, "A fuzzy diagnosis of multi-fault state based on information fusion from multiple sensors," *J. Vibroeng.*, vol. 18, pp. 2135–2148, May 2016.
[9] C. Li, J. L. de Oliveira, M. C. Lozada, D. Cabrera, V. Sanchez, and G. Zurita, "A systematic review of fuzzy formalisms for bearing fault diagnosis," *IEEE Trans. Fuzzy Syst.*, to be published. doi: 10.1109/TFUZZ.2018.2878200.
[10] C. Li, M.Cerrada, D. Cabrera, R. V. Sanchez, F. Pacheco, G. Ulutagay, and J. Valente de Oliveira, "A comparison of fuzzy clustering algorithms for bearing fault diagnosis," *J. Intell. Fuzzy Syst.*, vol. 34, no. 6, pp. 3565–3580, 2018.
[11] L. L. Cui, Y. Zhang, F. B. Zhang, J. Y. Zhang, and S. Lee, "Vibration response mechanism of faulty outer race rolling element bearings for quantitative analysis," *J. Sound Vibrat.*, vol. 364, pp. 67–76, Mar. 2016.
[12] H. Xue, H. Wang, P. Cheng, K. Li, and L. Song, "Automatic diagnosis method for structural fault of rotating machinery based on distinctive frequency components and support vector machines under varied operating conditions," *Neurocomputing*, vol. 116, no. 20, pp. 326–335, Sep. 2013.
[13] H. Wang, B. Ren, L. Song, and L. Cui, "A novel weighted sparse representation classification strategy based on dictionary learning for rotating machinery," *IEEE Trans. Instrum. Meas.*, to be published. doi: 10.1109/TIM.2019.2906334.
[14] Y. S. Hao, L. Y. Song, Y. L. Ke, H. Q. Wang, and P. Chen, "Diagnosis of compound fault using sparsity promoted-based sparse component analysis," *Sensors*, vol. 16, no. 6, p. 1307, Jun. 2017.
[15] K. Li, L. Su, J. J. Wu, H. Q. Wang, and P. Chen, "A rolling bearing fault diagnosis method based on variational mode decomposition and an improved kernel extreme learning machine," *Appl. Sci.*, vol. 7, no. 10, p. 1004, Sep. 2017.
[16] H. T. Xue, Z. X. Li, H. Q. Wang, and P. Chen, "Intelligent diagnosis method for centrifugal pump system using vibration signal and support vector machine," *Shock Vib.*, vol. 2014, Apr. 2014, Art. no. 407570.
[17] H. Xue, M. Wang, Z. Li, and P. Chen, "Fault feature extraction based on artificial hydrocarbon network for sealed deep groove ball bearings of in-wheel motor," in *Proc. Prognostics Syst. Health Manage. Conf. (PHM-Harbin)*, Jul. 2017, pp. 1–5. [Online]. Available: http://ieeexplore.ieee.org/document/8079189
[18] H. T. Xue, M. Wang, Z. X. Li, and P. Chen, "Sequential fault detection for sealed deep groove ball bearings of in-wheel motor in variable operating conditions," *J. Vibroeng.*, vol. 19, pp. 5947–5959, Apr. 2017.
[19] L. Song, H. Wang, and P. Chen, "Step-by-step fuzzy diagnosis method for equipment based on symptom extraction and trivalent logic fuzzy diagnosis theory," *IEEE Trans. Fuzzy Syst.*, vol. 26, no. 6, pp. 3467–3478, Dec. 2018.
[20] H. Wang, S. Li, L. Song, and L. Cui, "A novel convolutional neural network based fault recognition method via image fusion of multi-vibration-signals," *Comput. Ind.*, vol. 105, pp. 182–190, Feb. 2019.
[21] H. Wang, P. Wang, L. Song, B. Ren, and L. Cui, "A novel feature enhancement method based on improved constraint model of online dictionary learning," *IEEE Access*, vol. 7, pp. 17599–17607, Jan. 2019.
[22] Y. Hao, L. Song, L. Cui, and H. Wang, "A three-dimensional geometric features-based SCA algorithm for compound faults diagnosis," *Measurement*, vol. 134, pp. 480–491, Feb. 2019.
[23] L. Cui, X. Wang, Y. Xu, H. Jiang, and J. Zhou, "A novel switching unscented Kalman filter method for remaining useful life prediction of rolling bearing," *Measurement*, vol. 135, pp. 678–684, Mar. 2019.
[24] L. Cui, J. Huang, F. Zhang, and F. Chu, "HVSRMS localization formula and localization law: Localization diagnosis of a ball bearing outer ring fault," *Mech. Syst. Signal Process.*, vol. 120, pp. 608–629, Apr. 2019.
[25] L. Song, P. Chen, and H. Wang, "Vibration-based intelligent fault diagnosis for roller bearings in low-speed rotating machinery," *IEEE Trans. Instrum. Meas.*, vol. 67, no. 8, pp. 1887–1899, Aug. 2018.
[26] Z. Tang and X. G. Gao, "Research on radiant point identification based on discrete dynamic Bayesian network," *J. Syst. Simul.*, vol. 21, pp. 117–120, Sep. 2009.
[27] S. L. Liu, Y. P. Huang, and S. M. Liu, "Obstacle classification based on dynamic Bayesian network," *Softw. Guide*, vol. 17, pp. 25–27, Sep. 2018.
[28] Q. K. Xiao and R. Song, "Action recognition based on hierarchical dynamic Bayesian network," *Multimedia Tools Appl.*, vol. 77, pp. 6955–6968, Sep. 2018.
[29] J. L. Obuhuma, "Driver behaviour profiling using dynamic Bayesian network," *Int. J. Modern Edu. Comput. Sci.*, vol. 10, pp. 50–59, Apr. 2018.
[30] D. Codetta-Raiteri and L. Portinale, "Dynamic Bayesian networks for fault detection, identification, and recovery in autonomous spacecraft," *IEEE Trans. Syst., Man, Cybern. Syst.*, vol. 45, no. 1, pp. 13–24, Jan. 2015.
[31] B. Cai, Y. Liu, and M. Xie, "A dynamic-Bayesian-network-based fault diagnosis methodology considering transient and intermittent faults," *IEEE Trans. Autom. Sci. Eng.*, vol. 14, no. 1, pp. 276–285, Jan. 2017.
[32] H. W. Xie, J. Y. Shi, W. Lu, and W. W. Cui, "Dynamic Bayesian networks in electronic equipment health diagnosis," in *Proc. Prognostics Syst. Health Manage. Conf.*, to be published. [Online]. Available: http://ieeexplore.ieee.org/document/7819945, 2017.
[33] H. B. Zhang, Q. Zhang, J. J. Liu, and H. Z. Guo, "Fault detection and repairing for intelligent connected vehicles based on dynamic Bayesian network model," *IEEE Internet Things J.*, vol. 5, no. 4, pp. 2431–2440, Aug. 2018.
[34] L. Cui, X. Gong, J. Zhang, and H. Wang, "Double-dictionary matching pursuit for fault extent evaluation of rolling bearing based on the Lempel-Ziv complexity," *J. Sound Vib.*, vol. 385, pp. 372–388, Dec. 2016.
[35] H. Wang, Y. Yu, Y. Cai, X. Chen, L. Chen, and Q. Liu, "A comparative study of state-of-the-art deep learning algorithms for vehicle detection," *IEEE Intell. Transp. Syst. Mag.*, vol. 11, no. 2, pp. 82–95, Apr. 2019.
[36] L. Cui, J. Huang, H. Zhai, and F. Zhang, "Research on the meshing stiffness and vibration response of fault gears under an angle-changing crack based on the universal equation of gear profile," *Mech. Mach. Theory*, vol. 105, pp. 554–567, Nov. 2016.
[37] L. Cui, X. Wang, H. Wang, and N. Wu, "Improved fault size estimation method for rolling element bearings based on concatenation dictionary," *IEEE Access*, vol. 7, pp. 22710–22718, 2019.
[38] D. Wang, X. Zhao, L.-L. Kou, Y. Qin, Y. Zhao, and K.-L. Tsui, "A simple and fast guideline for generating enhanced/squared envelope spectra from spectral coherence for bearing fault diagnosis," *Mech. Syst. Signal Process.*, vol. 122, pp. 754–768, May 2019.
[39] A. Stief, J. Ottewill, J, Baranowski, "A PCA-two stage Bayesian sensor fusion approach for diagnosing electrical and mechanical faults in induction motors," *IEEE Trans. Ind. Electron.*, to be published.
[40] K. Li, X. Ping, H. Wang, P. Chen, and Y. Cao, "Sequential fuzzy diagnosis method for motor roller bearing in variable operating conditions based on vibration analysis," *Sensors*, vol. 13, pp. 8013–8041, May 2013.
[41] K. Li, P. Chen, and S. M. Wang, "An intelligent diagnosis method for rotating machinery using least Squares mapping and a fuzzy neural network," *Sensors*, vol. 12, pp. 5919–5939, May 2012.
[42] X. D. Sun, C. Hu, J. Zhu, S. Wang, W. Zhou, Z. Yang, G. Lei, K. Li, B. Zhu, and Y. Guo, "MPTC for PMSMs of EVs with multi-motor driven system considering optimal energy allocation," *IEEE Trans. Magn.*, to be published.
[43] P. Weber, D. Theilliol, C. Aubrun, and A. Evsukoff, "Increasing effectiveness of model-based fault diagnosis: A dynamic Bayesian network design for decision making," *IFAC Proc.*, vol. 39, pp. 90–95, Aug. 2007.
[44] X. G. Gao, *Discrete Dynamic Bayesian Networks Inference and Its Application*. Beijing, China: National Defense Industry Press, 2016, pp. 44–95.
[45] J. G. Shi and X. G. Gao, "Direct calculation inference algorithm for discrete dynamic Bayesian network," *Syst. Eng. Electron.*, vol. 27, pp. 1626–1630, Sep. 2015.
[46] W. Fan, Y. X. Li, K. L. Tsui, and Q. Zhou, "A noise resistant correlation method for period detection of noisy signals," *IEEE Trans. Signal Process.*, vol. 66, no. 7, pp. 2700–2710, Jul. 2018.
[47] H. C. Wang, "Research on Bayesian formula and Bayesian statistics," *J. Chongqing Univ. Sci. Technol.*, vol. 12, pp. 203–205, May 2010.
[48] J. L. Zhu, Z. D. Zhang, and F. Pan, "Fault identification for missing data systems with a dynamic Bayesian network approach," *Inf. Control*, vol. 42, pp. 499–505, May 2013.

[49] Hu, X. Wang, G. Ma, R.N, "Complex network in vulnerability based on dynamic Bayesian network," *Fire Control Command Control*, vol. 42, pp. 5–9, Sep. 2017.
[50] W. J. Qu, Z. L. Xu, and Y. W. Yuan, "Air intelligence radar battle damage assessment based on dynamic Bayesian networks," *Tactical Missile Technol.*, vol. 5, pp. 93–100, Sep. 2016.
[51] X. H. Zhu, S. M. Cui, N. Shi, and Y. L. Wen, "Grey prediction model of motor reliability of electric vehicle," *Electr. Mach. Control.*, vol. 16, pp. 42–46, May 2012.
[52] J. Wang, J. Zhang, and B. F. Hu, "Optimal class-dependent discretization-based fine-grain hypernetworks for classification of microarray data," *J. Shanghai Jiao Tong Univ*, vol. 37, no. 12, pp. 1856–1862, Jun. 2013.
[53] C. G. Enright, M. G. Madden, and N. Madden, "Bayesian networks for mathematical models: Techniques for automatic construction and efficient inference," *Int. J. Approx. Reasoning*, vol. 54, no. 2, pp. 323–342, Sep. 2013.
[54] Y. C. Qin, M. M. Dong, F. Zhao, and L. Gu, "Suspension semi-active control of vehicles based on road profile classification," *J. Northeastern Univ. (Natural Sci.)*, vol. 37, pp. 1138–1143, Aug. 2016.

HONGTAO XUE (M'19) was born in Nanyang, China, in 1978. He received the Ph.D. degree in mechatronic engineering from the Graduate School of Bioresources, Mie University, Japan, in 2014. He is currently with the School of Automotive and Traffic Engineering, Jiangsu University, China. His research interests include fault diagnosis for plant machinery, and information and signal processing.

JIAWEN ZHOU was born in Hengyang, China, in 1996. He received the B.S. degree in automobile service from the Qingdao University of Technology. He is currently pursuing the master's degree in vehicle engineering with Jiangsu University. His research interest includes the fault diagnosis of in-wheel motors.

ZHENYU CHEN was born in Nantong, China, in 1993. He received the B.S. degree from the School of Automotive and Traffic Engineering, Jiangsu University, where he is currently pursuing the master's degree in vehicle engineering. His research interests include state monitoring and intelligent fault diagnosis systems.

ZHONGXING LI was born in Shanghai, China, in 1963. He received the Ph.D. degree in vehicle engineering from the Jiangsu University of Science and Technology, Zhenjiang, China, in 2007. He is currently a Professor with the School of Automobile and Traffic Engineering, Jiangsu University, China. His research interests include fault diagnosis and fault tolerant control, vehicles running simulation, and control quality.